Microtubule Structure at Improved Resolution†

Patricia Meurer-Grob,‡ Jérôme Kasparian,§ and Richard H. Wade*

Institut de Biologie Structurale (CEA/CNRS), 41 rue Jules Horowitz, 38027 Grenoble, France

Received February 19, 2001; Revised Manuscript Received April 16, 2001

ABSTRACT: Microtubule architecture can vary with eukaryotic species, with different cell types, and with the presence of stabilizing agents. For in vitro assembled microtubules, the average number of protofilaments is reduced by the presence of sarcodictyin A, epothilone B, and eleutherobin (similarly to taxol) but increased by taxotere. Assembly with a slowly hydrolyzable GTP analogue GMPCPP is known to give 96% 14 protofilament microtubules. We have used electron cryomicroscopy and helical reconstruction techniques to obtain three-dimensional maps of taxotere and GMPCPP microtubules incorporating data to 14 Å resolution. The dimer packing within the microtubule wall is examined by docking the tubulin crystal structure into these improved microtubule maps. The docked tubulin and simulated images calculated from "atomic resolution" microtubule models show tubulin heterodimers are aligned head to tail along the protofilaments with the β subunit capping the microtubule plus end. The relative positions of tubulin dimers in neighboring protofilaments are the same for both types of microtubule, confirming that conserved lateral interactions between tubulin subunits are responsible for the surface lattice accommodation observed for different microtubule architectures. Microtubules with unconventional protofilament numbers that exist in vivo are likely to have the same surface lattice organizations found in vitro. A curved "GDP" tubulin conformation induced by stathmin-like proteins appears to weaken lateral contacts between tubulin subunits and could block microtubule assembly or favor disassembly. We conclude that lateral contacts between tubulin subunits in neighboring protofilaments have a decisive role for microtubule stability, rigidity, and architecture.

Microtubules are key actors in the cytoskeleton of eukaryotic cells where they play important roles in organizing the spatial distribution of organelles during interphase and of chromosomes throughout cell division. They can be extremely stable as in cilia and flagella or very dynamic as in the mitotic spindle. Microtubules are ~25 nm diameter hollow tubes with walls made from tubulin heterodimers stacked head to tail at 8 nm intervals to form "protofilaments" that run lengthwise along the wall. These protofilaments associate laterally with an ~0.9 nm offset such that tubulin subunits in neighboring protofilaments describe a 12 nm pitch, left-handed, helical pathway around the microtubule. Microtubule architecture in living cells depends on the number of protofilaments, usually 13, but a very wide range is possible (*1*−*6*).

The α and β tubulin subunits have very similar sequences and three-dimensional structures (*7*). By treating the subunits as identical, the nomenclature *N*:*S* provides a simple classification of different microtubule structures via the two most prominent surface lattice features, the number of protofilaments (*N*) and the number of lateral helices (*S*, called S-start helices). In vitro, pure tubulin can assemble into many microtubule polymorphs with a wide range of protofilament numbers, typically in the range $10 \leq N \leq 16$, and with $2 \leq S \leq 4$. Microtubules can accommodate this wide range of protofilament numbers by a rotational adjustment of their surface lattice, giving long-pitch superhelical protofilaments as confirmed by electron cryomicroscopy. The conservation of the lateral contacts between protofilaments has been proposed as the driving force for this accommodation process (*8*−*12*).

In 1998, an atomic resolution structural model of the tubulin heterodimer was obtained by electron crystallography of taxol-stabilized zinc sheets (*7*). Since protofilaments in zinc sheets and microtubules have the same longitudinal packing, this gives a putative model of the inter- and intradimer contacts along the protofilaments. Neighboring protofilaments are aligned antiparallel in zinc sheets and parallel in microtubules, making it more difficult to detect possible lateral contacts between microtubule protofilaments. This question was addressed by docking zinc sheet protofilaments into a 20 Å resolution map of microtubules obtained by electron cryomicroscopy (*13*). A major structural feature involved in lateral interactions between tubulin subunits was found to be the M loop situated between β strand S7 and α helix H9 (structural features of the β subunit are shown in Figures 3 and 5) (*7*, *13*−*15*). In β tubulin, this loop is influenced by the antimitotic drug taxol that binds to a nearby site, occupied in α tubulin by an eight-residue insert in the loop between S9 and S10. The stabilization of

† Work supported by grants from the Association pour la Recherche sur le Cancer and from the Région Rhône-Alpes. R.H.W. acknowledges the support offered by a NATO Collaborative Research Grant.

* Corresponding author: e-mail, wade@ibs.fr; telephone, 33(0)-438784024; fax, 33(0)438785494.

‡ Present address: Molecular and Cell Biology Department, University of California, Berkeley, CA 94720-3200.

§ Present address: LASIM, Universite Claude Bernard Lyon 1, 43 Boulevard du 11 Novembre 1918, 69622 Villeurbanne, France.

10.1021/bi010343p CCC: $20.00
Published on Web 06/13/2001

microtubules by taxol blocks cell division, leading to the use of this drug for chemotherapy of certain forms of cancer (*16*). In addition, taxol has the interesting property of modifying microtubule architecture by reducing the average number of protofilaments (*17*−*19*).

Microtubules have a remarkable dynamical polarity, as witnessed by the different growth and shrinkage rates of their two ends (*20*). In many cells, microtubules grow outward from the microtubule organizing center (MTOC)[1] toward the cell membrane with the fast growing (plus) end leading and with the minus end remaining embedded in the MTOC. These networks, and the polar distribution of microtubules in the mitotic spindle, provide pathways for dynein and kinesin, allowing these ATP-dependent microtubule motors to participate in cell division and to engage in intracellular transport and organization. Both motor proteins can detect the underlying structural polarity of microtubules and move in specific directions with unerring accuracy (*21*). The kinesin motor domain interacts specifically with tubulin, and "decoration" with the kinesin motor domain has been used to determine the surface lattice organization of microtubules using electron microscopy: identical tubulin subunits are aligned along the lateral helices; this is known as the B lattice (*22*−*24*). As a result, interprotofilament contacts involve identical tubulin subunits with the important proviso that the B lattice has complete helical continuity only for an even number of lateral "monomer" helices (*22*, *25*). Consequently, for the 13 protofilament, 3 start (13:3) microtubules usually found in eukaryotic cells, there will be α to β contacts between a single pair of protofilaments. This "seam" is most likely a direct consequence of the microtubule growth process with tubulin dimers adding endwise onto sheets that protrude from the microtubule extremity (*26*, *27*). It is an open question as to whether the seam has a functional role such as providing a "weak link" facilitating microtubule disassembly.

Subtle differences between α and β tubulin are implicated in the relationship between the structural and dynamic polarity of microtubules. Considerable efforts have been made to relate the tubulin dimer orientation to microtubule polarity leading to the current picture with β tubulin capping the microtubule plus end and α tubulin the minus end (*28*−*30*). Microtubule assembly requires the presence of GTP at the E (exchangeable) site on the β subunit, and hydrolysis accompanies microtubule growth so that microtubules are mostly made up of "GDP tubulin" with the growing end capped by GTP tubulin, probably limited to the endmost tubulin dimer. During microtubule growth, the α subunit of an incoming tubulin dimer will interact with the in situ β subunit and provoke GTP hydrolysis. The α tubulin capped minus end will behave differently since GTP in α tubulin is buried within the αβ interface and is neither exchangeable (N site) and nor hydrolyzable. Microtubules formed in the presence of the slowly hydrolyzable analogue GMPCPP are more stable than GDP microtubules, suggesting that GDP tubulin is required for microtubule disassembly (*31*). GDP tubulin is thought to have a natural curved conformation as witnessed by the ring-like structures produced when microtubules disassemble. In addition, some proteins, such as stathmin, interfere with microtubule assembly either by sequestering tubulin or by destabilizing microtubules. The presence of stathmin at the microtubule plus end could block microtubule growth by inducing protofilament curvature similar to the conformation of the two tubulin dimers complexed to a stathmin-like domain observed recently by X-ray crystallography (*32*).

We first determined how a number of stabilizing agents, epothilone B, sarcodictyin A, eleutherobin (for a brief description of these drugs, see refs *33* and *34* and references cited therein), taxotere, and GMPCPP, influence microtubule architecture. We then used electron cryomicroscopy and helical reconstruction techniques to obtain three-dimensional maps of two different microtubule architectures, incorporating data to 14 Å resolution: (i) 14:3 microtubules (not strictly helical) assembled in the presence of GMPCPP and (ii) 15:4 microtubules (strictly helical) assembled in the presence of the antimitotic drug taxotere.

The dimer packing within the microtubule wall and the putative longitudinal and lateral interactions between tubulin subunits are examined by docking the crystal structure of the tubulin dimer into our improved microtubule maps. We compare the lateral contact geometry between tubulin subunits for the two microtubule lattices. Simulated images calculated from "atomic resolution" microtubule models are used to confirm the docked tubulin dimer orientation within the microtubule protofilaments. Finally, we suggest that the crystal structure of tubulin associated with a stathmin-like domain indicates how a curved tubulin conformation could weaken lateral contacts between tubulin subunits and either block microtubule assembly or favor protofilament separation during plus end disassembly.

EXPERIMENTAL PROCEDURES

Tubulin was prepared and purified as described (*35*). Control microtubules were assembled from pure tubulin in the presence of excess GTP in assembly buffer as described (*19*). Similarly, microtubules were assembled from pure tubulin at 10 μM with an additional 20 μM of the following drugs: epothilone B, sarcodictyin A, eleutherobin, and taxotere. GMPCPP microtubules were assembled as described (*31*). Specimens were prepared for electron cryomicroscopy as described previously (*19*). Preliminary data were obtained using a Philips CM200 with a LaB_6 source and a liquid nitrogen cooled Gatan 626H side-entry stage. Micrographs were recorded under low dose conditions at a nominal electron optical magnification of 38000×. The lengths of each type of microtubule were measured directly on photographic prints for each assembly condition and the results expressed as a percentage of the total length of all microtubules.

For 3D image reconstruction, images of 14:3 and 15:4 microtubules, selected using their characteristic moiré pattern contrast (*9*, *10*), were digitized using a modified Optronics P1000 scanner with a raster corresponding to about 3.25 Å at the specimen. The quality of the digitization was later checked using a ZEISS SCAI scanner. Preliminary image

[1] Abbreviations: ATP, adenosine 5′-triphosphate; CCF, cross-correlation coefficient; CTF, contrast transfer function; FOM, figure of merit; GMPCPP, guanylyl α,β-methylenediphosphonate; GDP, guanosine 5′-diphosphate; GTP, guanosine 5′-triphosphate; GMPCPP microtubule, microtubules assembled in the presence of GMPCPP (a similar notation is used for tubulin and for other nucleotides and drugs); MTOC, microtubule organizing center.

treatment was carried out, as described, on Silicon Graphics workstations using SUPRIM software (*36*) and some in-house procedures. Fourier transforms were calculated for 512 by 4096 pixel regions (Supporting Information, Figure 1). Layer line data were extracted using in-house procedures, and the MRC helical program package (*37*) was used for tilt correction, alignment, etc. Preliminary reconstructions to 18 Å resolution were calculated using layer lines within the first CTF maximum.

Further images were recorded at a nominal 40000× magnification using the liquid helium cooled stage installed on the JEOL3000FEG in the laboratory of Y. Fujiyoshi, Kyoto. A total of 500 images of GMPCPP microtubules were recorded over a defocus range of 1−2 μm. The defocus was calculated using 512 by 512 pixel regions extracted from the carbon background visible at the edges of the micrographs using a procedure similar to that adopted by Morgan et al. (*38*). Sometimes, we were able to verify the defocus against the value found within the ice layer over a hole. Only images with negligible astigmatism were retained. The measured defocus is accurate to ±2%. For each defocus a theoretical CTF (weak amplitude, weak phase object approximation) was calculated to find the best fit with the maxima and minima positions of the experimental data, and the radial intensity fall off was compensated by a envelope function equivalent to that due to the angular illumination aperture (*39*). This procedure gives an estimate for the CTF of each image (Supporting Information, Figures 2 and 3).

Ten images, corresponding to about 22 000 tubulin heterodimers, were selected for the final GMPCPP microtubule reconstruction. For each microtubule image, layer lines were extracted from the 512 by 4096 Fourier transform, for near and far sides, at positions corresponding to multiples of vertical heights Z_N, Z_S ($Z = lZ_N + kZ_S$, l and k are integers) even if there was no clearly visible "diffraction" peak. In addition, background "layer lines" were extracted at intermediate positions. A similar procedure was adopted for the seven micrographs selected from the 72 image data set obtained for taxotere microtubules. The layer line data were averaged over the complete data set:

$$F_{av}(n,R,Z) = \sum_i F_i(n,R,Z)K_i(R,Z)/\sum_i K_i^2(R,Z)$$

where $F_{av}(n,R,Z)$ is the average Fourier coefficient along R for the nth order Bessel component on the layer line at height Z above the equator. F_i is the coefficient for the ith member of the data set and $K_i(R,Z)$ is the value of the CTF at the radial position R on the Z layer line; see, for example, ref *40*. Each averaged layer line was compared to the averaged background and a local figure of merit (FOM) calculated along each layer line Z (Supporting Information, Figure 4):

$$\mathrm{FOM}(n,R,Z) = |\sum_i F_i(n,R,Z)|/\sum_i |F_i(n,R,Z)|$$

The summation runs over the data set, $i = 1, N$. Note that N

Table 1: Stabilizing Agents Influence Microtubule Architecture[a]

protofilaments	11	12	13	14	15	16
control	0	0	35	55	10	0
taxol	3	60	35	2	–	–
eleutherobin	1	57	41	2	–	–
sarcodictyin A	0	43	51	5	–	–
epothilone B	0	22	67	11	1	0
taxotere	–	2	30	38	26	4
GMPCPP	–	0	3	96	–	–

[a] Microtubules assembled in the presence of GTP (control), antimitotic drugs, and GMPCPP are observed by electron cryomicroscopy and classed according to the number of protofilaments as assessed from the characteristic image contrast (*8*, *9*). For each assembly condition, the values are expressed as percentages of the total length and rounded off to the nearest integer. For example, zero indicates a value less than or equal to 0.5 whereas dashes indicate no observed microtubules.

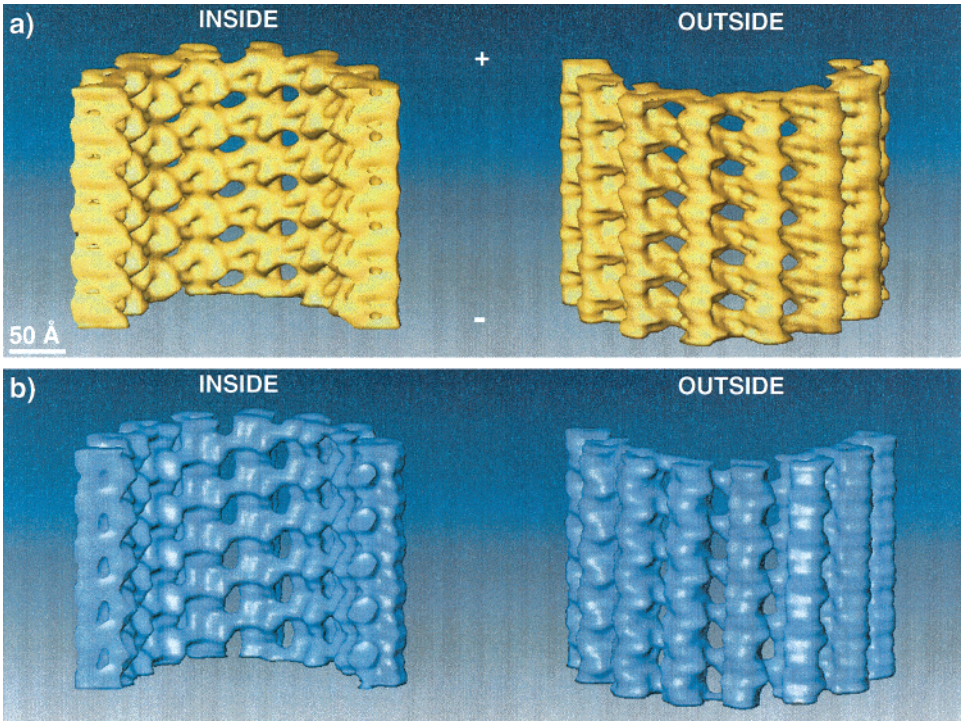

FIGURE 1: Three-dimensional structures of (a) GMPCPP microtubules (yellow) and (b) taxotere microtubules (blue). The isosurface representations are cut lengthwise to show the inner (left) and the outer (right) surfaces of the microtubules (plus end upward).

= 20 for GMPCPP microtubules, and $N = 14$ for taxotere microtubules, counting near and far data from one image as two data sets. Layer line peaks are then selected on the criteria that their value is greater than $3\sigma_n$ (standard deviation of the local noise) and that their FOM is significantly greater than 0.5, corresponding to a highly acceptable phase error (*41*). 3D density maps are calculated using an in-house modification of the MRC Fourier−Bessel inversion program HLXFOUR (*37*).

The crystal structure (*7*) of the tubulin dimer (*T*) was docked into the 3D density map using a computational procedure developed in house (*42*) to obtain the position and orientation of *T* maximizing the cross-correlation coefficient

$$C = \sum_i (D_i - D_{av})(T_i - T_{av}) / [\sum_i (D_i - D_{av})^2 \sum_i (T_i - T_{av})^2]^{1/2}$$

where the summation covers the pixels $i = 1, N$ in a selected volume *D* of the density map (pixel values D_i, average D_{av}) and in the tubulin dimer (pixel values T_i, average T_{av}). The volume *T* is calculated from the tubulin structure PDB file at 14 Å resolution to match the resolution of the microtubule density map. Potential docking positions are located by initially fitting the atomic resolution model into the microtubule density map by eye. The extracted volume *D* includes the putative tubulin docking position. *C* is calculated for *D* covering a range of starting positions.

RESULTS

(a) Microtubule Surface Lattice in the Presence of Stabilizing Agents. Specimens were prepared for electron microscopy shortly after microtubule assembly in the presence of stabilizing agents as described in Experimental Procedures. We found that microtubules can be stable at room temperature for 10 days or more after assembly. Table 1 shows that epothilone B, sarcodictyin A, and eleutherobin behave similarly and, like taxol (*17*−*19*), favor microtubule populations with reduced numbers of protofilaments compared to the control assembly, suggesting that this group of drugs stabilizes microtubules by a similar mechanism. The presence of taxotere gives, on the average, microtubules with more protofilaments than the control assembly. Assembly in the presence of GMPCPP gives 96% of 14 protofilament microtubules. This highly defined microtubule population is unique for microtubule-stabilizing agents examined to date and implies that the nucleotide influences the lateral interactions between tubulin subunits in adjacent protofilaments.

On the basis of these results we decided to investigate the three-dimensional structures of microtubules with two distinctly different surface lattices: 14:3 microtubules assembled in the presence of GMPCPP that are not strictly helical and the 15:4, strictly helical, microtubules assembled with taxotere.

(b) Microtubule Structures. Figure 1 shows isosurface representations of three-dimensional reconstructions at about 14 Å resolution of (a) GMPCPP and (b) taxotere microtubules. As we expected, and verified on the computed Fourier transforms (Supporting Information, Figure 1), the α and β tubulin subunits are indistinguishable at this resolution. The outer surface views show parallel, compact

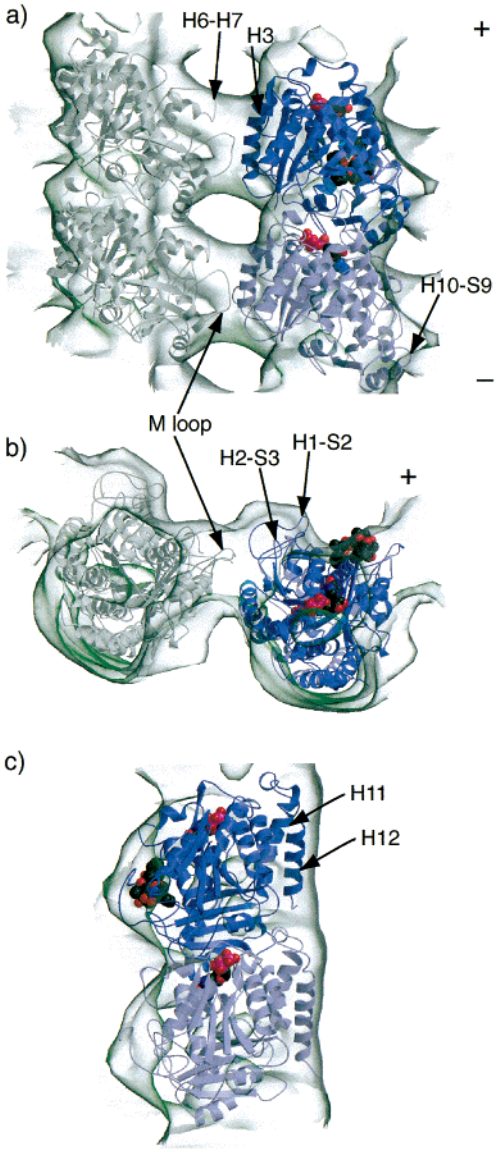

FIGURE 2: Tubulin crystal structure docked into the GMPCPP microtubule map (gray isodensity surface). The α and β subunits are shown respectively as lighter and darker blue ribbon representations. (a) Part of two neighboring protofilaments viewed from the microtubule outer surface. (b) End-on view of these protofilaments from the microtubule plus end. (c) Side view of a protofilament across the thickness of the microtubule wall.

protofilaments separated by deep grooves. The main contacts between protofilaments are at the bottom of the grooves with large windows (about 15 by 25 Å for taxotere, 15 Å by 20 Å for GMPCPP) giving direct access to the microtubule lumen. Each protofilament is shifted lengthwise by about 9 Å with respect to its neighbor. The outermost surface of the protofilaments is quite smooth and the inner surface rough. There is an ~40 Å repeat in the density distribution along the protofilaments corresponding to the spacing between the α and β tubulin subunits. As viewed from the outer surface, the right-hand sides of the protofilaments in GMPCPP and taxotere microtubules are quite similar (for GMPCPP microtubules there is one longer extension of density into the groove just above the windows). The left-hand sides are rather different: strongly indented with extensions into the interprotofilament region for GMPCPP, whereas for taxotere this side has smoother undulations.

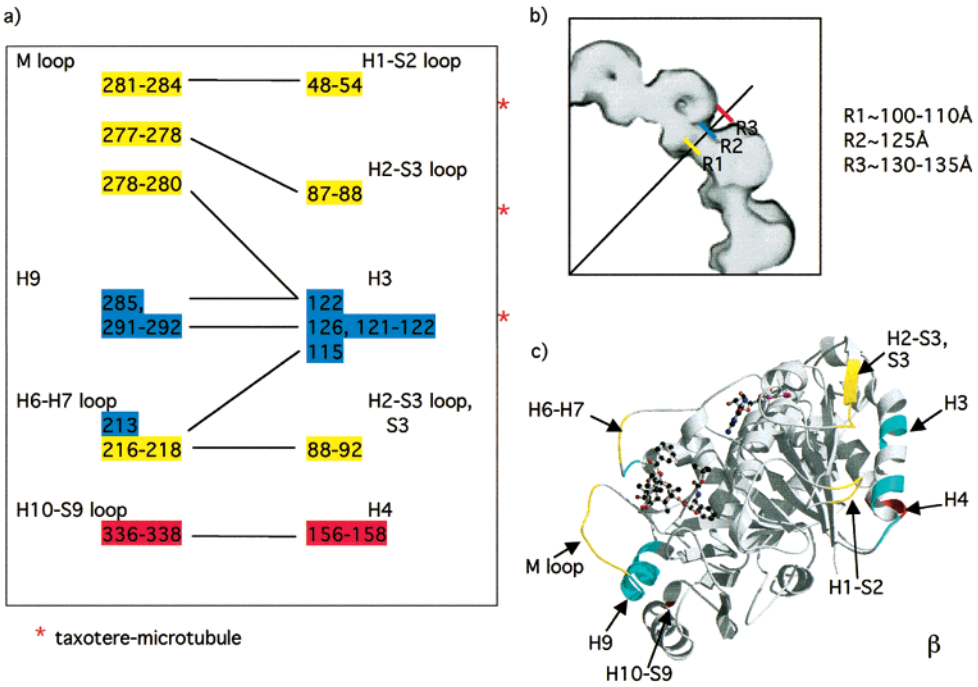

FIGURE 3: Putative lateral contacts between tubulin subunits in GMPCPP microtubules (stars for taxotere microtubules). (a) Residues are identified by the color code yellow, blue, and red according to their position in the groove between protofilaments as seen in (b) a cross section of part of the microtubule wall and in (c) the ribbon diagram of the β tubulin subunit viewed from the microtubule lumen.

GMPCPP microtubules appear to have more extensive interprotofilament contacts.

Figure 2 shows front, top, and side views of the tubulin dimer structure docked into the GMPCPP microtubule reconstruction as described in Experimental Procedures. The cross-correlation coefficient $C = 0.83$ (0.81 for taxotere) indicates the excellent quality of the docking. Visual inspection shows there are no overlapping subunits, no significant structural elements outside the isodensity surface, and no large empty spaces inside. The rough inner surface matches features such as the long H1−S2 loop. The longitudinal interfaces between subunits appear similar to those in the zinc sheet protofilaments as previously described and will not be discussed in detail (*7*).

We suppose lateral contacts between subunits in adjacent protofilaments are possible if (a) the carbon backbones of neighboring tubulin subunits are within 3−6 Å of each other and (b) the 3D reconstructions show significant density crossing the grooves between the protofilaments. Both reconstructions show connections at the bottom of the grooves between protofilaments where the M loop in one tubulin subunit interacts with H3 and loops H1−S2, H2−S3 in the neighboring subunit. The GMPCPP microtubule map suggests that lateral contacts may extend over a range of radii, as measured from the microtubule axis. The M loop and H1−S2 interact at a radius of 100−110 Å; at about 125 Å, the end of the M loop leading into H9 could contact the helix H3; further out, at a radius of 130−135 Å, there is a possible contact between loop H10−S9 and the C-terminal end of H4. Although H4 and the H10−S9 loop are not very close in the docked tubulin structures, the tubulin conformations may be different in taxol-stabilized zinc sheets and in GMPCPP microtubules. This is quite feasible since loop H10−S9 is close to the nucleotide binding site on the next subunit along the protofilament. The glycine-rich tubulin signature loop T4 (GGGTGS), at the N terminus of H4, interacts with the phosphates in the nucleotide so the position of H4 could depend on the nucleotide state. Another possibility concerns putative contacts between the H6−H7 loop and H3. Again, although these regions are rather far apart in docked tubulin neighbors, they could be influenced either by the nucleotide via loop T3 or by taxotere via H6 and H7. The possible lateral contacts just described are shown in Figure 3. It must be borne in mind that at the present stage we can only propose putative contact zones. Higher resolution microtubule reconstructions and an improved tubulin structure will be required to accurately identify specific interactions between individual side chains.

We have compared the relative positions of tubulin dimers in neighboring protofilaments, as docked for GMPCPP and taxotere microtubules, and find their positions match to within ±2 Å (Supporting Information, Figure 5). Since the precision of the independent docking process for the two maps at 14 Å resolution is expected to be about 3 Å (*43*), this indicates that the significantly different surface lattices of GMPCPP (14:3) and taxotere (15:4) microtubules have essentially the same interprotofilament contacts. We conclude that maintaining these lateral contacts is the essence of the accommodation process by which microtubules adapt to a wide range of protofilament numbers (*8*, *9*).

Atomic resolution models can be built using the tubulin dimer crystal structure and the helical parameters of the two types of microtubule. Projection maps calculated from these models are comparable to micrographs obtained by electron cryomicroscopy and show the moiré patterns and the arrow contrast expected for 14:3 and 15:4 microtubules (*44*). The arrows indicate the microtubule polarity and, together with the docking process described above, provide an unambiguous and independent determination of the tubulin dimer orientation within the protofilaments (Supporting Informa-

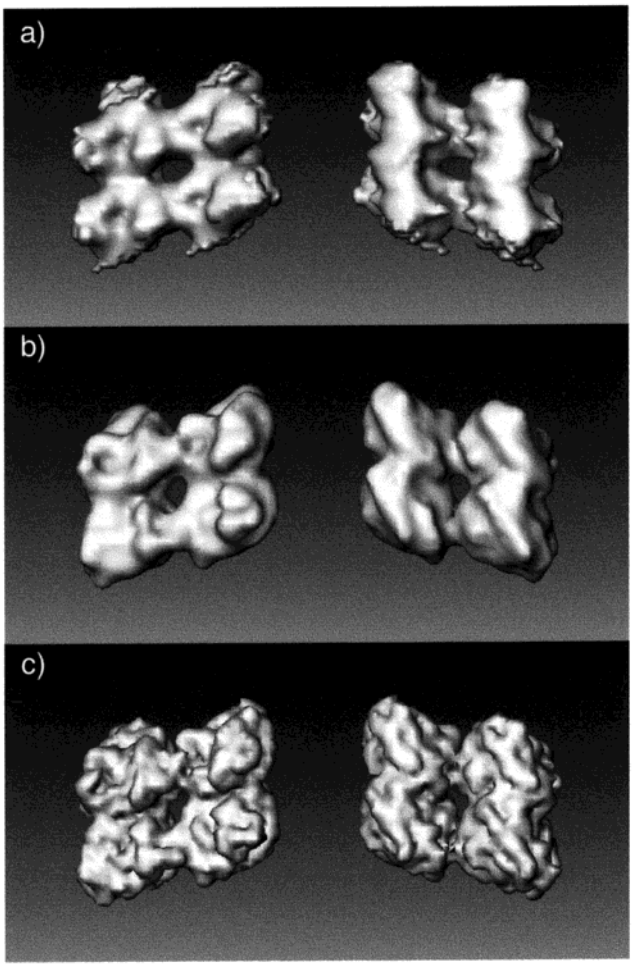

FIGURE 4: Experimental and computed structures of tubulin dimers in neighboring protofilaments. Isodensity surfaces viewed from the microtubule inside (left) and outside (right). Panels: (a) as seen in the 3D GMPCPP microtubule map, (b) computed at 15 Å resolution from the tubulin crystal structure, and (c) computed at 8 Å resolution.

tion, Figure 6). The β subunit caps the microtubule plus end, and the α subunit is at the minus end. In addition, the models provide a good estimate of the resolution required to visualize specific structural features. For example, Figure 4 shows two dimers, in neighboring protofilaments, generated at 15 Å (Figure 4b) and 8 Å (Figure 4c) resolution, respectively. The 15 Å resolution model shares many features on the outer and inner surface with the 3D reconstructions as seen in Figures 4a and 1. We believe the differences seen on the outer surface, corresponding mainly to helices H11 and H12, arise because a number of weaker reflections away from the azimuth are absent in our present data set.

DISCUSSION

Taxol, sarcodictyin A, epothilone B, and eleutherobin give long-term stability to in vitro assembled microtubules, and judging from their behavior in reducing the average numbers of protofilaments incorporated into microtubules, they appear to have similar effects on lateral interactions between tubulin subunits in adjacent protofilaments. Taxotere increases the average protofilament number, indicating that this drug must have different interactions within the taxol binding region of β tubulin. GMPCPP is unique in producing so many identical microtubules (96% 14 protofilament microtubules). The implication that the nucleotide influences lateral interactions between protofilaments is, at first site, surprising since the exchangeable site on the β subunit lies at the longitudinal interface between tubulin dimers along the protofilaments. However, several regions directly involved with nucleotide binding could possibly affect the position of helices or loops involved in lateral interactions (*13*, *15*).

Docking the atomic structure of the tubulin dimer into the 14 Å resolution microtubule maps gives an unambiguous orientation of the tubulin dimer within a protofilament and confirms the essential features of the longitudinal interactions between complementary surfaces of the tubulin subunits deduced from the zinc sheet structure (*7*, *13*−*15*). For GMPCPP microtubules the density between the protofilaments suggests lateral interactions over an extended thickness between protofilaments, in the range of 100−135 Å from the microtubule axis. The docking and a pseudo-atomic resolution microtubule model show that the tubulin dimer is aligned head to tail along protofilaments with the β subunit capping the microtubule plus end. This gives an independent, structure-based confirmation of microtubule polarity suggested by a variety of other methods (*28*−*30*). Essentially the same lateral interactions exist between tubulin subunits for two quite different microtubule architectures, supporting the proposal that these interactions are the driving force behind the accommodation mechanism that allows microtubules to adapt to a wide range of protofilament numbers in vivo as in vitro (*8*, *9*).

There are, indeed, many well-documented examples of organisms and cell types in which the usual 13 protofilament microtubules are replaced by microtubules with different numbers of protofilaments, and it has been established that β tubulin is particularly important for determining microtubule architecture (*45*). A good example is provided by the nematode *Caenorhabditis elegans*, which has microtubules with 11 protofilaments in most somatic cells apart from six touch receptor neurons containing 15 protofilament microtubules. The *mec-12* α tubulin and the *mec-7* β tubulin genes are highly expressed in the touch cells and give a cell-specific tubulin heterodimer (*46*, *47*). Mutations in either gene typically lead to touch-insensitive animals lacking 15 protofilament microtubules, but *mec-7* has been much more extensively studied (*4*). In Figure 5, the blue markers indicate, for the nematode β tubulins mec-7, ben-1, and tub-1, the residues differing from pig β tubulin. Only seven residues are unique to mec-7 β tubulin. Two of these, T127 and C293, are in regions involved in lateral contacts, and four other residues in the M loop differ from pig β tubulin. Savage et al. suggested in 1989 that the region between residues 260 and 300 is important for interactions between protofilaments (*4*). More recently, a systematic study of 45 mutations in *mec-7* has allowed sequence alterations to be correlated with mutant phenotypes (*48*). Three severe recessive alleles have mutations in the tubulin signature region and may fail to bind GTP. Many of the dominant mutations disrupt microtubule assembly, and the mutation sites, shown in green, were found in three clusters that were proposed to be important for longitudinal and lateral interactions between tubulin subunits within the microtubule wall. This is now strikingly confirmed by the structural results. Residues 171−188 (loop

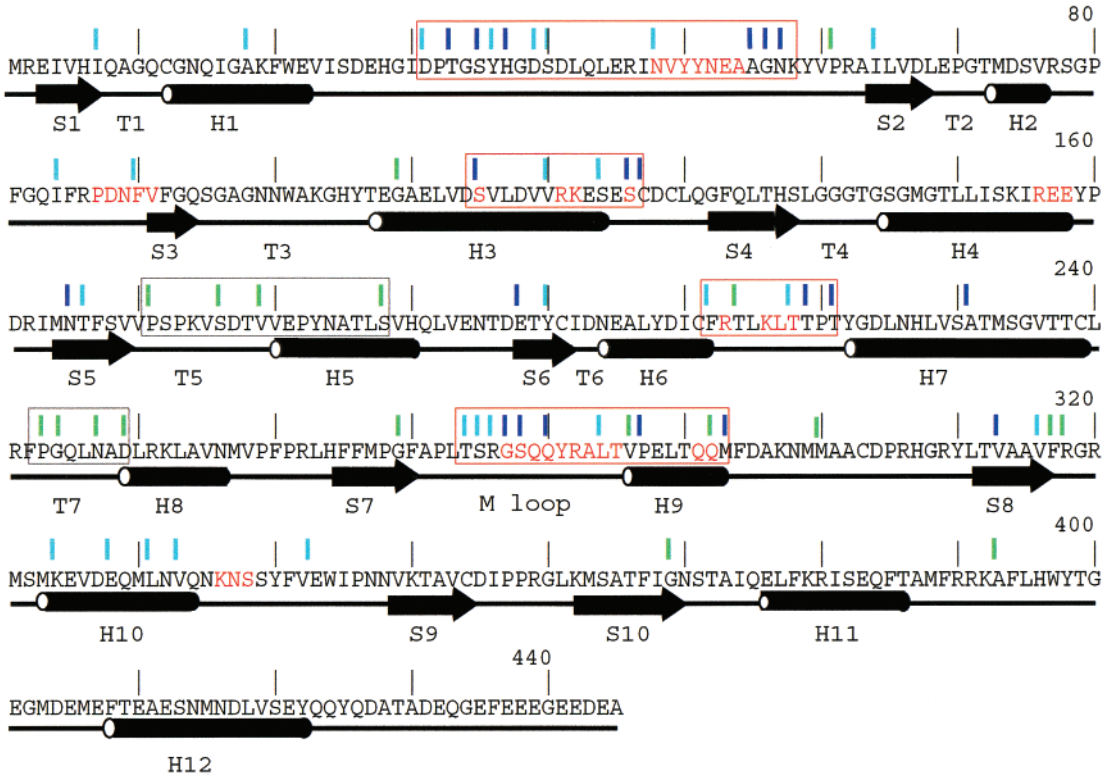

FIGURE 5: Sequence of pig β tubulin with corresponding structural features, β strands S, α helices H, and turns T. Residues involved in lateral contacts are shown in red. Blue tags indicate residues in *C. elegans*, mec-7, ben-1, and tub-1 β tubulins that differ from pig β tubulin. Light blue indicates similar residues and dark blue weakly similar and different residues. Green tags indicate mutation sites in severe domininant and semidominant alleles in mec-7 (*47*). The red and gray boxes outline respectively lateral and longitudinal contact regions with clusters of tagged residues.

T5 and helix H5) are involved in longitudinal contacts, residues 243−249 (loop T7) interact with the γ phosphate on the next tubulin subunit along the microtubule and are also involved in longitudinal contacts, and residues 286−318 are in the M loop region and are involved in lateral contacts.

The *tub-1* and *ben-1* β tubulins incorporated into the 11 protofilament microtubules in the other nematode somatic cells share a substitution of alanine for the usually invariant proline 287 at the beginning of H9 (*49*). Alanine scan mutagenesis of β tubulin in another organism, the yeast *Saccharomyces cerevisiae*, shows that lethal substitutions are mainly grouped in regions close to the longitudinal or lateral interfaces (*50*). A point mutation E288K in the *Drosophila* testes specific β2 tubulin gives defective tubule morphology both in vivo and in vitro (*51*). The remarkable cold stability of microtubules in two Antartic fish (*Notothenia coriiceps* and *Chionodraco rastrospinosus*) was recently discussed in terms of specific features in tubulin sequences (*52*). Unusual or unique residues at the molecular surface localize to the inside of the microtubule and to loops involved in lateral contacts. It was suggested that two such residues within the M loop, G280 and S285 in the β subunit, increase the loop flexibility and strengthen lateral interactions.

It is interesting that the β tubulin M loop is also involved in microtubule stabilization by the taxol family of drugs (*13*−*15*) and probably by the other drugs investigated here. Microtubules assembled in the presence of taxol have fewer protofilaments than those assembled with taxotere (Table 1), suggesting that the M loop has a specific conformation for each of these drugs. The most important difference between taxol and taxotere is at the end of the side chain connected to C13 in the taxane ring. At this position (C5′) taxol has an aromatic ring (AR3) and taxotere a *tert*-butyl group [O−C(CH_3)$_3$]. These may interact differently with H7, thereby modifying the interaction of the aromatic ring (AR2) with helix H1, loop S9−S10, and perhaps with β strand S7. This could lead to slightly different interactions of the M loop with the taxane rings in taxol and in taxotere, thereby modifying the position of the M loop so that it acts as an effector both for microtubule stability and for protofilament number. This is supported by the strong immobilization of the C13 side chain when taxol binds to the tubulin dimer whereas the taxane ring itself is immobile only when the dimer is incorporated into the microtubule wall (*53*). Note that taxol-resistant human ovarian cancer cells have β tubulins with mutations near the beginning of the M loop (P270V) and in the S9−S10 loop (A364T) (*54*).

GMPCPP microtubules also have greater stability compared to standard microtubules containing mainly GDP tubulin. Intuitively, the GMPCPP (GTP-like state) might be expected to strengthen lengthwise interactions along the protofilaments, giving another possibility for microtubule stabilization. However, our three-dimensional maps suggest that taxoids could favor strong but flexible contacts near the inner surface of the microtubule wall whereas GMPCPP microtubules appear to have more extensive lateral interactions across the groove between protofilaments. We note that, on one hand, GMPCPP microtubules are significantly more rigid than GDP and taxol microtubules (*55*−*60*) and that, on the other hand, the precisely defined number of protofilaments obtained during tubulin assembly in the presence

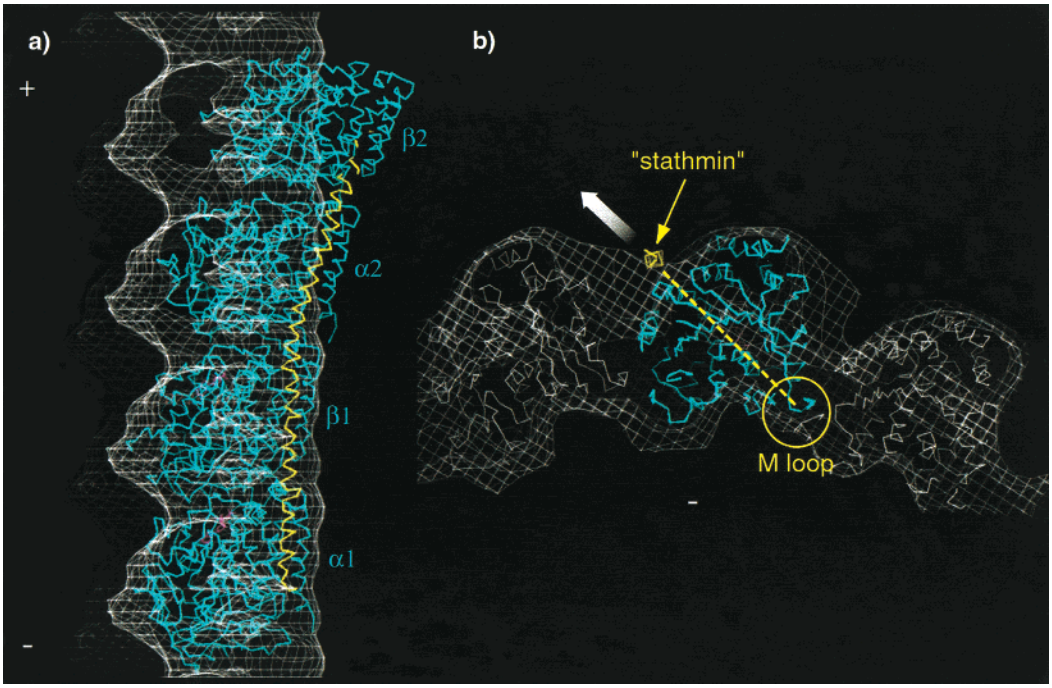

FIGURE 6: The curved configuration of tubulin dimers interacting with stathmin may weaken lateral contacts between protofilaments. The crystallographic structure of the complex between two tubulin dimers (the backbones of tubulin α1β1 and α2β2 are shown in blue) and a stathmin-like helical domain (yellow) from the neural protein RB3 (*32*) is fitted to the plus end of the GMPCPP microtubule map (chicken wire) with the α1 subunit at the docking position as shown in Figure 2. (a) Section across a protofilament showing the curved tubulin−stathmin complex peeling away from the microtubule wall. (b) End-on view looking from the minus end toward the microtubule plus end. The stathmin-like domain is offset into the groove between protofilaments and pulls tubulin subunits directly away (white arrow) from the M loop contacts with subunits in the neighboring protofilament.

of GMPCPP unambiguously shows the strong influence of the tubulin nucleotide state on lateral interactions between protofilaments. This leads to the suggestion that lateral interactions are the important factor in microtubule stability and that an increased number of contacts between protofilaments may explain the greater rigidity of GMPCPP microtubules.

Many results suggest that tubulin has a straight "GTP-like" form and a bent GDP-like form corresponding to the curved protofilaments that peel off the plus end of microtubules and to tubulin rings observed when microtubules depolymerize (*61*, *62*). In this view, it is the lateral interactions within the microtubule wall that constrain GDP tubulin to hold a straight conformation until released during disassembly. A curved conformation has recently been observed in the crystal structure of two GDP tubulin dimers complexed with an α helical stathmin-like domain from the neural protein RB3 (*32*). It was also shown that, when placed at the microtubule plus end, the helical stathmin-like domain is offset to one side of a protofilament. Figure 6 shows that the tubulin−stathmin-like crystal structure, fitted to a microtubule plus end, rather than just coiling the protofilament directly away from the microtubule wall, curves the protofilament extremity so as to pull directly on the M loop contact in the neighboring protofilament. This could specifically hinder lateral contacts required for microtubule growth or, alternatively, favor disassembly by weakening the inter-protofilament contacts that stabilize microtubules.

In conclusion, lateral contacts between tubulin subunits in neighboring protofilaments appear as the key factor for defining the microtubule surface lattice and number of protofilaments, for microtubule assembly and disassembly, for microtubule stabilization by "taxol-like" antimitotic drugs, and for determining microtubule rigidity.

ACKNOWLEDGMENT

It is a pleasure to acknowledge the hospitality of Yoshi Fujiyoshi during our visit to Kyoto to use his wonderful microscope equipped with a field emission gun and a highly stable, liquid helium cooled, specimen stage. We are indebted to Ken Downing and Eva Nogales for communicating the refined tubulin coordinates and to Marcel Knossow for the coordinates of the tubulin−stathmin-like domain complex. We have benefited in several respects from exchange visits with Pier Luigi Bellon and Salvatore Lanzavecchia, our friends in Milan, and we thank them for help concerning modifications to our Optronics scanner and also for allowing us to use interpolation software developed in Milan. We acknowledge exchange visits with Ken Downing during this project and for ongoing discussions. We thank Frédéric Metoz for his essential contribution to the computating facility and for customized software. Eric Thouvenin gave help in using his cross-correlation programs. We are grateful to Tony Hyman for GMPCPP and to Dr. K. C. Nicolau for epothilone B, sarcodictyin A, and eleutherobin. Taxotere was a kind gift from Dr. J. L. Fabre.

SUPPORTING INFORMATION AVAILABLE

(1) Images of microtubules in vitreous ice and computed diffraction pattern; (2) experimental contrast transfer function curve, fit to theoretical curve, and averaged contrast transfer profile for the GMPCPP microtubule data set; (3) data for images used for reconstructions, defocus and source size used for CTF correction, layer-line positions for unit reciprocal

lattice vectors, and phase residuals; (4) layer-line data for GMPCPP and taxotere microtubules with corresponding background noise and figure of merit (FOM) as defined in Experimental Procedures; (5) relative positions of tubulin dimers as docked into neighboring protofilaments for GMPCPP and taxotere microtubules; (6) microtubule polarity and tubulin dimer orientation from computed images using the atomic structure of tubulin and the microtubule helical parameters. This material is available free of charge via the Internet at http://pubs.acs.org.

REFERENCES

1. Afzelius, B. A., Bellon, P. L., and Lanzavecchia, S. (1990) *J. Cell Sci. 95*, 207−217.
2. Burton, P. R., Hinkley R. E., and Pierson, G. B. (1975) *J. Cell Biol. 65*, 227−233.
3. Eichenlaub-Ritter, U., and Tucker, J. B. (1984) *Nature 307*, 60−62.
4. Savage, C., Hamelin, M., Culotti, J. G., Coulson, A., Albertson, D. G., and Chalfie, M. (1989) *Genes Dev. 3*, 670−881.
5. Tilney, L. G., Bryan, J., Bush, D. J., Fujiwara, K., Mooseker, M. S., Murphy, D. B., and Snyder, D. H. (1973) *J. Cell Biol. 59*, 267−275.
6. Tucker, J. B., Milner, M. J., Currie, D. A., Muir, J. W., Forrest, D. A., and Spencer, M.-J. (1986) *Eur. J. Cell Biol. 41*, 279−289.
7. Nogales, E., Wolf, S. G., and Downing, K. A. (1998) *Nature 391*, 199−203.
8. Wade, R. H., Chrétien, D., and Job, D. (1990) *J. Mol. Biol. 212*, 775−786.
9. Chrétien, D., and Wade, R. H. (1991) *Biol. Cell 71*, 161−174.
10. Wade, R. H., and Chrétien, D. (1993) *J. Struct. Biol. 110*, 1−27.
11. Chrétien, D., Flyvbjerg, H., and Fuller, S. D. (1998) *Eur. Biophys. J. 27*, 490−500.
12. Wade, R. H., Meurer-Grob, P., Metoz, F., and Arnal, I. (1998) *Eur. Biophys. J. 27*, 446−454.
13. Nogales, E., Whittaker, M., Milligan, R. A., and Downing, K. A. (1999) *Cell 96*, 79−88.
14. Nogales, E., and Downing, K. A. (1998) *Curr. Opin. Cell Biol. 10*, 16−22.
15. Amos, L. A., and Löwe, J. (1999) *Chem. Biol. 6*, R65−R69.
16. Rowinsky, E. K., Cazenave, L. A., and Donnehower, R. C. (1990) *J. Natl. Cancer Inst. 82*, 1247−1259.
17. Andreu, J. M., Bordas, J., Diaz, J. F., Garcia de Ancos, J., Gil, R., Medrano, F. J., Nogales, E., Pantos, E., and Towns-Andrews, E. (1992) *J. Mol. Biol. 226*, 169−184.
18. Andreu, J. M., Diaz, J. F., Gil, R., de Pereda, J. M., Garcia de Lacomba, M., Peyrot, V., Briand, C., Towns-Andrews, E., and Bordas, J. (1994) *J. Biol. Chem. 269*, 31784−31792.
19. Arnal, I., and Wade, R. H. (1995) *Curr. Biol. 5*, 900−908.
20. Mitchison, T., and Kirschner, M. (1984) *Nature 312*, 237−242.
21. Bloom, G. S., and Endow, S. A. (1995) *Motor Proteins I: Kinesin, Protein Profile 1*, Academic Press, New York.
22. Amos, L. A., and Klug, A. (1974) *J. Cell Sci. 14*, 523−549.
23. Song, Y.-H., and Mandelkow, E. (1993) *Proc. Natl. Acad. Sci. U.S.A. 90*, 1671−1675.
24. Harrison, B. C., Marchese-Ragona, S. P., Gilbert, S. P., Cheng, N., Steven, A. C., and Johnson, K. A. (1993) *Nature 362*, 72−75.
25. Wade, R. H., Horowitz, R., and Milligan, R. A. (1995) *Proteins 23*, 502−509.
26. Erickson, H. P. (1974) *J. Cell Biol. 60*, 153−167.
27. Chrétien, D., Fuller, S. D., and Karsenti, E. (1995) *J. Cell Biol. 129*, 1311−1328.
28. Mitchison, T. J. (1993) *Science 261*, 1044−1047.
29. Hirose, K., Fan, J., and Amos, L. A. (1995) *J. Mol. Biol. 251*, 329−333.
30. Fan, J., Griffith, A. D., Lockhart, A., and Cross, R. A. (1996) *J. Mol. Biol. 259*, 325−330.
31. Hyman, A. A., Salser, S., Dreschel, D. N., Unwin, N., and Mitchison, T. J. (1992) *Mol. Biol. Cell 3*, 1155−1167.
32. Gigant, B., Curmi, P. A., Martin-Barbey, C., Charbaut, E., Lachkar, S., Lebeau, L., Siavoshian, S., Sobel, A., and Knossow, M. (2000) *Cell 102*, 809−816.
33. Cowden, G. J., and Paterson, I. (1997) *Nature 387*, 238−239.
34. Holmes, A. (1997) *Nature 390*, 560−561.
35. Asnes, C. F., and Wilson, L. (1979) *Anal. Biochem. 98*, 64−73.
36. Schroeter, J. P., and Bretaudière, P. (1996) *J. Struct. Biol. 116*, 131−137.
37. Crowther, R. A., Henderson, R., and Smith, J. M. (1996) *J. Struct. Biol. 116*, 9−16.
38. Morgan, D. G., Owen, C., Melanson, L. A., and DeRosier, D. A. (1995) *J. Mol. Biol. 249*, 88−110.
39. Wade, R. H. (1992) *Ultramicroscopy 46*, 145−156.
40. Unwin, N. (1993) *J. Mol. Biol. 229*, 1101−1124.
41. Mimori, Y., Yamashita, I., Murata, K., Fujiyoshi, Y., Yonekura, K., Toyashima, C., and Namba, K. (1995) *J. Mol. Biol. 249*, 69−87.
42. Thouvenin, E., and Hewat, E. (2000) *Acta Crystallogr. D56*, 1350−1357.
43. Baker, T. S., and Johnson, J. E. (1996) *Curr. Opin. Struct. Biol. 6*, 585−594.
44. Chrétien, D., Kenney, J. M., Fuller, S. D., and Wade, R. H. (1996) *Structure 4*, 1031−1040.
45. Raff, E. C., Fackenthal, J. D., Hutchens, J. A., Hoyle, H. D., and Turner, F. R. (1997) *Science 275*, 70−73.
46. Savage, C., and Chalfie, M. (1991) *Cell Motil. Cytoskel. 18*, 159−163.
47. Fukushiga, T., Siddiqui, Z. K., Chou, M., Culotti, J. G., Gogonea, C. B., Siddiqui, S. S., and Hamelin, M. (1999) *J. Cell Sci. 112*, 395−403.
48. Savage, C., Xue, Y., Mitani, S., Hall, D., Zakhary, R., and Chalfie, M. (1994) *J. Cell Biol. 107*, 2165−2175.
49. Driscoll, M., Dean, E., Reilly, E. Bergholz, E., and Chalfie, M. (1989) *J. Cell Biol. 109*, 2293−3003.
50. Reijo, R. A., Cooper, E. M., Beagle, G. J., and Huffaker, T. C. (1994) *Mol. Biol. Cell 5*, 29−43.
51. Rudolph, J. E., Kimble, M., Hoyle, H. D., Subler, M. A., and Raff, E. C. (1987) *Mol. Cell. Biol. 7*, 2231−2242.
52. Detrich H. W., Parker, S. A., Williams, R. C., Nogales, E., and Downing, K. H. (2000) *J. Biol. Chem. 275*, 37038−37047.
53. Nicholov, R., Kingston, D. G. I., Chordia, M. C., and DiCosmo, F. (1997) *FEBS Lett. 405*, 73−76.
54. Giannakakou, P., Sackett, D. L., Kang, Y.-K., Zhan, Z., Buters, J. T. M., Fojo, T., and Poruchynsky, M. S. (1997) *J. Biol. Chem. 272*, 17118−17125.
55. Mickey, B., and Howard, J. (1995) *J. Cell Biol. 130*, 909−917.
56. Venier, P., Maggs, A. C., Carlier, M.-C., and Pantaloni, D. (1994) *J. Biol. Chem. 269*, 13353−13360.
57. Dye, R. B., Fink, S. P., and Williams, R. C. (1993) *J. Biol. Chem. 268*, 6847−6850.
58. Gittes, F., Mickey, B., Nettleton, J., and Howard, J. (1993) *J. Cell Biol. 120*, 923−934.
59. Felgner, H., Frank, R., and Schliwa, M. (1996) *J. Cell Sci. 109*, 509−516.
60. Kurachi, M., Hoshi, M., and Tashiro, H. (1995) *Cell Motil. Cytoskel. 30*, 221−228.
61. Mandelkow, E.-M., Mandelkow, E., and Milligan, R. A. (1991) *J. Cell Biol. 114*, 977−991.
62. Melki, R., Carlier, M.-F., Pantaloni, D., and Timasheff, S. N. (1989) *Biochemistry 28*, 9143−9152.

BI010343P